Tailoring intrinsic chirality in a two-dimensional planar waveguide grating via quasibound states in the continuum

Dandan Zhang,[1] Tingting Liu,[2,3] Linlin Lei,[4] Weimin Deng,[1] Tongbiao Wang,[1] Qinghua Liao,[1] Wenxing Liu,[1,*] Shuyuan Xiao,[2,3,†] and Tianbao Yu[1,‡]

[1]*School of Physics and Materials Science, Nanchang University, Nanchang 330031, China*
[2]*School of Information Engineering, Nanchang University, Nanchang 330031, China*
[3]*Institute for Advanced Study, Nanchang University, Nanchang 330031, China*
[4]*Jiujiang Vocational and Technical College, Jiujiang 332007, China*

(Received 9 February 2024; revised 8 April 2024; accepted 11 April 2024; published 2 May 2024)

The strong chiral light-matter interaction is crucial for various important fields such as chiral optics, quantum optics, and biomedical optics, driving a quest for the extreme intrinsic chirality assisted by ultra-high-quality (Q-) factor resonances. In this quest we propose a straightforward method to achieve extreme intrinsic chirality in lossless planar structures by manipulating the quasi-BIC through in-plane perturbation. The temporal coupled-mode theory is employed to derive the conditions necessary for achieving maximal intrinsic chirality. The quasi-BIC should be excited within the transparent spectral range of the structure and couple with x- and y-polarized waves with the same intensity but a phase difference of $\pi/2$. For an illustration, a planar chiral dielectric dimeric waveguide grating is designed that strongly interacts with left circularly polarized light while decoupling from right circularly polarized light through in-plane symmetry engineering. Furthermore, by adjusting the magnitude of the in-plane asymmetry, we can independently manipulate the Q factors of the chiral quasi-BIC while maintaining near unity circular dichroism. Our results provide a simple yet powerful paradigm for achieving extreme intrinsic chirality on an easily manufacturable platform, which may have potential applications in chiral emission, chiral sensing, and enantiomer separation.

DOI: 10.1103/PhysRevB.109.205403

I. INTRODUCTION

Chirality refers to the geometric property of an object that cannot be superimposed onto its mirror image by rotation or translation [1]. In the context of optics, chiral objects interacting with left or right circularly polarized (LCP, RCP) light can induce chiroptical effects, including optical activity and circular dichroism. Optical devices with a strong chiroptical response are crucial in various applications, such as chiral molecule sensing [2], enantiomer selection [3], and quantum optics [4]. However, the chiral light-matter interactions in natural materials are typically very weak, making it challenging to detect the resulting optical response for small amounts. In recent years, benefiting from the unprecedented flexibility for design, various chiral nanophotonic structures have been considered to generate strong chiral optical responses, such as the helices [5,6], twisted cross structures [7,8], and multilayered structures [9,10]. Nevertheless, due to absorption and scattering losses, these structures only support low-Q-factor optical responses, which inevitably hampers their potential applications, relying on strong chiral light-matter interactions.

Recently, the emergence of bound states in the continuum (BICs) has provided a viable alternative to enhance the strength of chiral light-matter interactions, owing to their unique ability to confine energy [11–15]. BICs are localized photonic eigenstates embedded in the radiation continuum, which can be considered as a resonance with zero linewidth or an infinite Q factor due to the energy being perfectly confined within the system [16,17]. Typically, the limited size of the structure, material losses, and other external perturbations can cause BICs to come into Fano resonance with finite but high Q factors, which are referred to as quasi-BICs [18–24]. The quasi-BICs with significantly high Q factors have been applied in areas such as low-threshold lasing [25–27], efficient nonlinear optical processes [28–32], and unidirectional emission [33–36]. Importantly, when a quasi-BIC acquires intrinsic chirality, the resulting chiral quasi-BIC can generate strong chiroptical effects accompanied with high Q factors. For example, a bilayer twisted structure could efficiently control chirality due to the absence of all mirror symmetries [37]. The maximum intrinsic chirality can be achieved by introducing out-of-plane perturbations to control the coupling of quasi-BIC with circularly polarized waves, as exemplified by pairs of ellipse dimers with a small out-of-plane distance [38–40], tilted etch twisted dimers [34], and slanted trapezoid nanoholes in dielectric film [41]. However, the introduced out-of-plane perturbations resort to three-dimensional sophisticated geometries, which is challenging to conventional 2D photolithography manufacturing techniques.

In this work we propose a straightforward method to achieve the extreme intrinsic chirality in planar structures

*liuwenxing@ncu.edu.cn
†syxiao@ncu.edu.cn
‡yutianbao@ncu.edu.cn

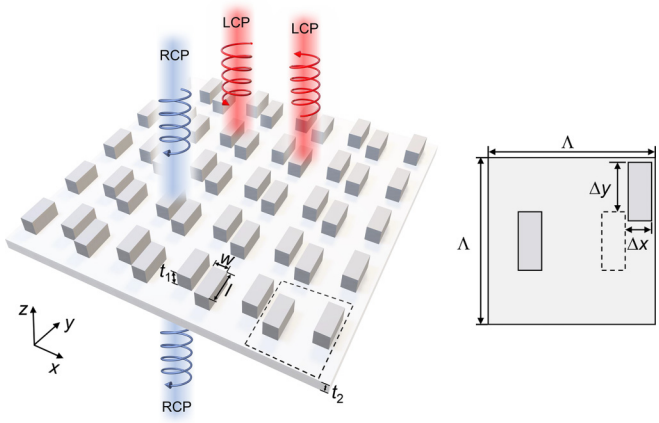

FIG. 1. The schematic configuration of the planar chiral waveguide grating composed of periodic dimeric rectangular bars arranged on a waveguide layer. The incident light is assumed to be a plane wave propagating along the z direction.

through manipulating the quasi-BIC *via* in-plane perturbation. Based on the temporal coupled-mode theory (CMT), we derive the conditions necessary for achieving maximal intrinsic chirality: (i) the quasi-BIC resonance should occur within the transparent spectral range of the structure, (ii) the dissipation loss must be negligible, and (iii) the quasi-BIC must couple with x- and y-polarized waves with exactly the same intensity but with a phase difference of $\pi/2$. As an example, we designed a planar waveguide grating comprising a dimeric grating and a waveguide layer that fulfill the above conditions. Through in-plane symmetry engineering, a quasi-BIC corresponding to the high-Q guided resonance (GR) is excited, which exhibits strong interaction with LCP light while decoupling from RCP light. The simulation results demonstrate 99.5% transmittance and reflectance for RCP and LCP waves, respectively. Moreover, by adjusting the magnitude of the in-plane asymmetry, we can independently manipulate the Q factors of the chiral quasi-BIC while maintaining nearly unity circular dichroism (CD).

II. THEORETICAL ANALYSIS OF MAXIMUM CD

Figure 1 schematically shows the concept and configuration of maximal intrinsic chirality. Circularly polarized lights are normally incident on the configuration, in which the RCP light is fully transmitted with same handedness and the LCP light is completely reflected. We start by discussing the necessary condition for maximal chirality based on Jones matrix analysis. Here the transmission matrices between the circular and linear polarization bases are related as [42]

$$T_{\text{circ}} = \begin{pmatrix} t_{\text{RR}} & t_{\text{RL}} \\ t_{\text{LR}} & t_{\text{LL}} \end{pmatrix} = \frac{1}{2}\begin{pmatrix} (t_{xx}+t_{yy})+i(t_{xy}-t_{yx}) & (t_{xx}-t_{yy})-i(t_{xy}+t_{yx}) \\ (t_{xx}-t_{yy})+i(t_{xy}+t_{yx}) & (t_{xx}+t_{yy})-i(t_{xy}-t_{yx}) \end{pmatrix}, \tag{1}$$

where the first and second subscripts refer to the transmitted and incident waves, R and L denote the right-handed circularly polarized wave (RCP) and left-handed circularly polarized wave (LCP), and x and y represent the two orthogonal linearly polarized waves. The transmission CD is defined as $\text{CD} = |t_{\text{RR}}|^2 + |t_{\text{LR}}|^2 - |t_{\text{RL}}|^2 - |t_{\text{LL}}|^2$. The maximal CD requires that the chiral structures completely transmit one helicity of circularly polarized incident light but completely reflect circularly polarized incident light with the opposite handedness. For maximal CD, we can consider following two cases. Case (1): the CD originates from anisotropy-induced polarization conversion, which is usually referred to as "false chirality" [41,43–48]. We can readily prove the maximal CD follows a Jones matrix in the linear and circular polarization bases:

$$T_{\text{lin}} = \begin{pmatrix} t_{xx} & t_{xy} \\ t_{yx} & t_{yy} \end{pmatrix} = \frac{e^{i\varphi}}{2}\begin{pmatrix} 1 & i \\ i & -1 \end{pmatrix}, \quad T_{\text{circ}} = e^{i\varphi}\begin{pmatrix} 0 & 1 \\ 0 & 0 \end{pmatrix}. \tag{2}$$

Case (2): only one helicity of circular polarization incidence can be transmitted without polarization conversion, which is considered as "true chirality" or "intrinsic chirality" [41]. In this case, the maximal CD follows a Jones matrix in the linear and circular polarization bases,

$$T_{\text{lin}} = \begin{pmatrix} t_{xx} & t_{xy} \\ t_{yx} & t_{yy} \end{pmatrix} = \frac{e^{i\varphi}}{2}\begin{pmatrix} 1 & -i \\ i & 1 \end{pmatrix}, \quad T_{\text{circ}} = e^{i\varphi}\begin{pmatrix} 1 & 0 \\ 0 & 0 \end{pmatrix}, \tag{3}$$

where φ is an arbitrary phase shift through the chiral structure. Due to limitations in applications caused by false chirality in important fields such as chiral emission and polarized photodetection, we focus solely on intrinsic chirality in this study.

To describe the light transmission and reflection through the chiral structure, we can exploit the $\boldsymbol{S}$ matrix, which relates the incoming and outgoing wave coefficients in the basis of linear polarizations, given as

$$\boldsymbol{S} = \begin{pmatrix} r_{1xx} & t_{2xx} & r_{1xy} & t_{2xy} \\ t_{1xx} & r_{2xx} & t_{1xy} & r_{2xy} \\ r_{1yx} & t_{2yx} & r_{1yy} & t_{2yy} \\ t_{1yx} & r_{2yx} & t_{1yy} & r_{2yy} \end{pmatrix}, \tag{4}$$

where the r_{mjk} and t_{mjk} are the reflection and transmission coefficients of j-component under incident k-component light from structure sides m. Here we resort to phenomenological CMT to derive the reflection and transmission coefficients in Eq. (4) and give the physically meaningful parameter condition for maximal intrinsic chirality in Eq. (3). In our CMT, we only consider the chiral structure hosting a single resonance. The dynamic equations for the amplitude A of the resonance mode can be written as [42,49,50]

$$\frac{dA}{dt} = (-i\omega_0 - \gamma)A + \boldsymbol{\kappa}^T \boldsymbol{a}, \tag{5}$$

$$\boldsymbol{b} = \boldsymbol{S}\boldsymbol{a} = \boldsymbol{C}\boldsymbol{a} + \boldsymbol{M}A, \tag{6}$$

where ω_0 and γ are the center frequency and the decay rate of the resonance, respectively; $\boldsymbol{a} = [a_{1x} \quad a_{2x} \quad a_{1y} \quad a_{2y}]^T$ and $\boldsymbol{b} = [b_{1x} \quad b_{2x} \quad b_{1y} \quad b_{2y}]^T$ represent the amplitudes of incoming and outgoing waves, where the subscripts denote the side of the structure and polarizations; $\boldsymbol{C}$ is the scattering matrix for the background transmission and reflection through the structure; and $\boldsymbol{\kappa} = [m_{1x} \quad m_{2x} \quad m_{1y} \quad m_{2y}]^T$ describes the coupling between the resonance and the incoming waves. According to Lorentz reciprocity, the matrix $\boldsymbol{M}$ is related to $\boldsymbol{\kappa}$ and is given by $\boldsymbol{M} = \boldsymbol{\kappa}$. Naturally, the single resonance is coupled to all linearly polarized waves on both sides of the structure. The stationary solution of Eqs. (5) and (6) determines the $\boldsymbol{S}$ matrix from Eq. (4) as

$$\boldsymbol{S} = \boldsymbol{C} - \frac{\boldsymbol{M}\boldsymbol{\kappa}^T}{i(\omega - \omega_0) - \gamma}. \tag{7}$$

From Eq. (7) we can obtain all the reflection and transmission coefficients in Eq. (4) by the model parameters. To achieve the intrinsic chirality describing in Eq. (3), the structure usually needs to have C_4 rotational symmetry with respect to the z axis [42]. However, the intrinsic chirality in C_4-symmetric structure is very weak, especially for a two-dimensional plane configuration [51,52]. Interestingly, the intrinsic chirality in Eq. (3) could be satisfied when the structure hosts a resonance in a spectral range where the background is perfectly transparent. In this case the scattering matrix of the background is given by

$$\boldsymbol{C} = \begin{pmatrix} 0 & 1 & 0 & 0 \\ 1 & 0 & 0 & 0 \\ 0 & 0 & 0 & 1 \\ 0 & 0 & 1 & 0 \end{pmatrix}. \tag{8}$$

According to energy conservation and time-reversal symmetry, we have [53]

$$\boldsymbol{C}\boldsymbol{\kappa}^* = -\boldsymbol{M}, \tag{9}$$

$$\boldsymbol{M}^*\boldsymbol{M} = 2\gamma. \tag{10}$$

From Eqs. (9) and (10), we can obtain the coupling parameters on different sides of the structure: $m_{2x} = -m_{1x}^*$, $m_{2y} = -m_{1y}^*$, and $|m_{1x}|^2 + |m_{2x}|^2 + |m_{1y}|^2 + |m_{2y}|^2 = 2\gamma$. Due to Lorentz reciprocity, we consider the transmission matrix only from side 1 of the structure,

$$T_{\text{lin1}} = \begin{pmatrix} t_{1xx} & t_{1xy} \\ t_{1yx} & t_{1yy} \end{pmatrix} = \begin{pmatrix} 1 + \frac{|m_{1x}|^2}{i(\omega-\omega_0)-\gamma} & \frac{|m_{1x}||m_{1y}|e^{i\Delta\Phi}}{i(\omega-\omega_0)-\gamma} \\ \frac{|m_{1x}||m_{1y}|e^{-i\Delta\Phi}}{i(\omega-\omega_0)-\gamma} & 1 + \frac{|m_{1y}|^2}{i(\omega-\omega_0)-\gamma} \end{pmatrix}, \tag{11}$$

where $\Delta\Phi$ is phase difference between the coupling parameters m_{1x} and m_{1y}. From Eq. (11) we can obtain the necessary condition for the maximal intrinsic chirality in Eq. (3): $|m_{1x}| = |m_{1y}|$ and $\Delta\Phi = \pi/2$. The transmission matrix for circular polarization waves is then written as

$$T_{\text{circ}} = \begin{pmatrix} 1 & 0 \\ 0 & 1 + \frac{\gamma}{i(\omega-\omega_0)-\gamma} \end{pmatrix}, \tag{12}$$

where the maximal intrinsic chirality in the structure is achieved at the resonant frequency of $\omega = \omega_0$.

The above analysis concludes the necessary condition to realize the maximal intrinsic chirality in a structure: the resonance should occur in the spectral range of structure transparency, the dissipation in the structure material can be negligible, and the structure must couple with the x-polarized and y-polarized waves satisfying the given condition: $|m_{1x}| = |m_{1y}|$ and $\Delta\Phi = \pi/2$.

III. DESIGN OF PLANAR WAVEGUIDE GRATING WITH MAXIMUM INTRINSIC CHIRALITY

To fulfill the physical conditions as discussed above, a planar chiral waveguide grating consisting of periodic dimeric rectangular bars arranged on a waveguide layer is designed, as illustrated in Fig. 1. The distance between the centers of the two rectangular bars along the x direction is $\Lambda/2$ at the original position. The in-plane symmetry of the structure is broken by moving one of the rectangular bars, and the distance of the move along the x and y directions is denoted as Δx and Δy, respectively. The presence of the waveguide layer breaks the structural symmetry in the z-axis direction, forming a planar chiral structure. Such a planar structure can be manufactured using conventional photolithography techniques [54–57].

In our design, the transparent background in the desired wavelength is achieved by virtue of the Fabry-Perot interference. Here the structure is made entirely of silicon nitride (Si_3N_4, the permittivity is 4.08), and each unit cell is characterized by a period $\Lambda = 600$ nm; width, length, and thickness of rectangular bars are $w = 135$ nm, $l = 148$ nm, and $t_1 = 205$ nm, respectively; and waveguide layer thickness is $t_2 = 165$ nm. For achieving maximum intrinsic chirality, one needs to precisely control the coupling between the resonant mode and the incoming waves. In the following, we present a step-by-step design of such a resonant mode starting from BICs and carefully enable their equivalent coupling with x- and y-polarized waves through in-plane symmetry engineering. To capture a resonant mode, we exploit the engineered Brillouin zone folding-induced quasi-BIC. The first Brillouin zone (FBZ) of the structure is shown in Fig. 2(a). The blue and red boxes represent FBZs with and without perturbations, respectively. The blue shaded region indicates that the FBZ has been halved in the x direction due to the doubling of the period in the x direction. The momentum properties, i.e., the dispersion relation branches $\omega - nk$ in usual terms, are simulated with the commercial finite-element software COMSOL MULTIPHYSICS. In the simulations, the Floquet periodic boundary conditions are applied to a single unit cell, and the perfectly matched layers are used in the z direction. Here, we focus on a transverse-magnetic (TM)-like eigenmode in the waveguide layer. When $\Delta x = 0$ nm and $\Delta y = 0$ nm, the grating degenerates to a half-period grating along the x direction with $\Lambda' = \Lambda/2$, and its band corresponds to the red line in Fig. 2(b). It can be observed that the TM-like mode is below the light line (gray), indicating that the mode behaves as guided mode and cannot couple with the external incident light due to wave-vector mismatch. While introducing a period perturbation along the x direction by moving one of the rectangular bars along the x or y direction, the grating period became Λ, and its band (blue) is folded from the band of the half-period structure (red). Then, the guided mode rises to the

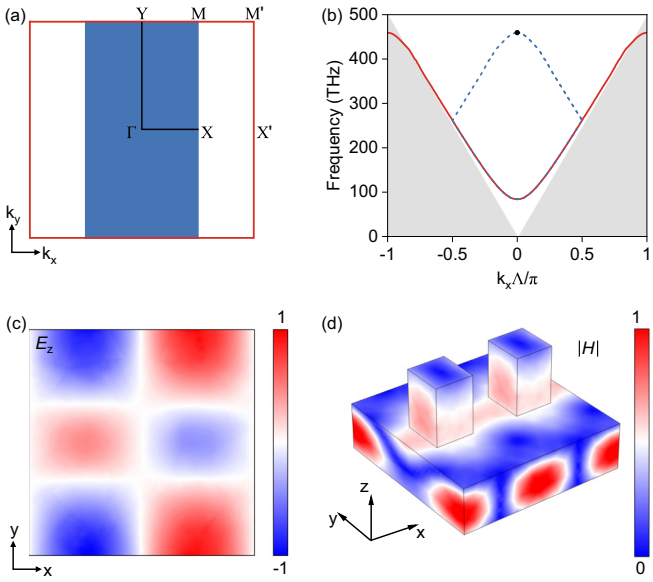

FIG. 2. (a) The first Brillouin zone of the structure. (b) The band structure of eigenmodes simulated with unit- (blue) and half- (red) period boundary; the light cone is represented a gray shaded area. (c) The eigenelectric field distribution with z component (E_z) at the Γ point. (d) The eigenmagnetic field distribution ($|H|$) at the Γ point.

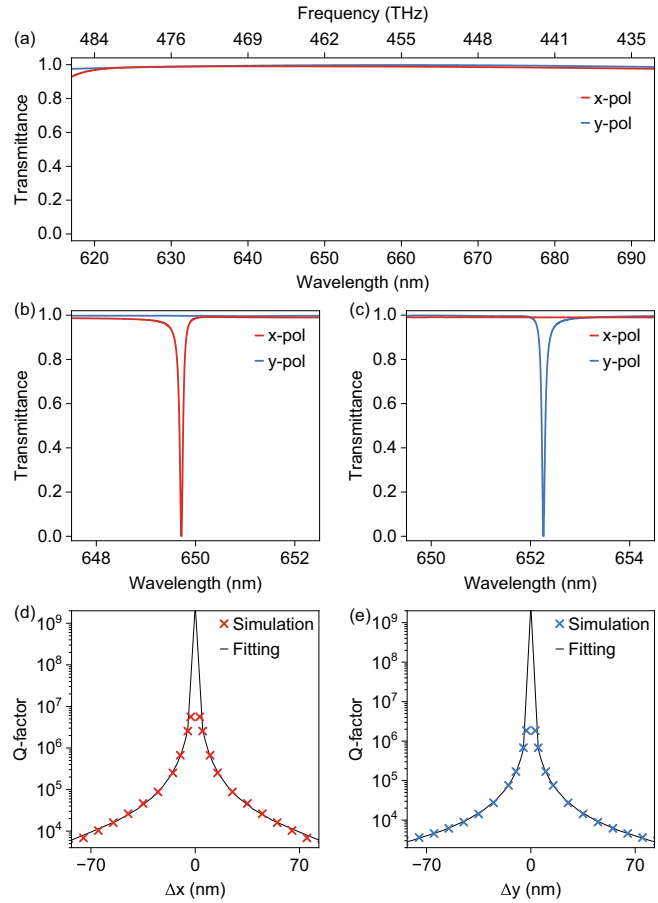

FIG. 3. The transmittance spectra under normal-incident, linearly polarized light for (a)$\Delta x = 0$ nm and $\Delta y = 0$ nm, (b) $\Delta x = 70$ nm and $\Delta y = 0$ nm, (c) $\Delta x = 0$ nm and $\Delta y = 45$ nm. The Q factors of the quasi-BIC mode as a function of (d) Δx and (e) Δy.

Γ point above the light line and couples with the external incident light, turning into GR. Since the GR is born from a small geometric perturbation, the coupling of the guided mode with the external incident light can be considered as a GR-assisted quasi-BIC.

The corresponding electromagnetic field distributions at the Γ point is shown in Figs. 2(c) and 2(d), respectively. As illustrated in Fig. 2(c), the z component of the electric field exhibits an odd symmetry under a 180° rotation around the z axis. The symmetries of the quasi-BIC can be tracked in the language of group theory by the irreducible representation B_1 mode of the point group C_{2v}. The selection rules show that the B_1 mode can radiate into free space in different polarization directions by introducing different perturbations [37,58,59]. When one of the rectangular bars moves along the x direction, the breaking of the symmetry along the x direction will introduce a leaky channel coupled to the continuum for x-polarized light, while for the rectangular bar moving along the y direction the structure lacks any in-plane mirror symmetries, other than in-plane inversion (C_2) symmetry, which will lead to the y-polarized light exhibiting a leaky resonance. Here, the magnetic field ($|H|$) suggests that the guided mode is strongly localized in the waveguide layer, as shown in Fig. 2(d).

To visualize the GR-assisted quasi-BIC, the transmissions through structure for different values of geometric perturbation are shown in Figs. 3(a)–3(c). For normal-incident linearly polarized light, the structure with $\Delta x = 0$ nm and $\Delta y = 0$ nm is perfectly transparent in the range of the concerned wavelengths. As shown in Fig. 3(a), the transmittance spectra show a wideband total-transmission Fabry-Perot background. Following the selection rules, we can manipulate the quasi-BIC radiation to different polarization directions by moving one of the rectangular bars along the x or y directions. Figures 3(b) and 3(c) illustrate the transmittance spectra of the structure for the normal-incident linearly polarized lights when $\Delta x = 70$ nm and $\Delta y = 45$ nm, respectively. When one of the rectangular bars moves along the x direction, the x-polarized light leads to a leaky resonance in the transmissive Fabry-Perot background [Fig. 3(b)]. In contrast, when the rectangular bar only moves along the y direction, the y-polarized light results in a leaky resonance [Fig. 3(c)]. Furthermore, Figs. 3(d) and 3(e) illustrate the Q factors as a function of Δx and Δy, respectively. The Q factors of the quasi-BIC resonance experience a dramatic increase as Δx or Δy decreases and diverges to infinity near $\Delta x = 0$ nm or $\Delta y = 0$ nm. According to the signature of quasi-BICs, its Q factor approximately follows an inversely quadratic law of asymmetric perturbations [13], i.e., $Q_x = \alpha/\Delta x^2$ and $Q_y = \beta/\Delta y^2$, where α and β present the different sensitivities of quasi-BIC resonance to Δx and Δy. This relation is verified by fitting results in Figs. 3(d) and 3(e) with the sensitivity factors of $\alpha = 4.22 \times 10^7$ and $\beta = 1.67 \times 10^7$. Meanwhile, the amplitudes of quasi-BIC resonance coupling to x and y polarization are proportional to the square root of the Q factor, i.e., $|m_x| \sim 1/\sqrt{Q_x}$ and $|m_y| \sim 1/\sqrt{Q_y}$. And therefore, the equivalent coupling ($|m_x| = |m_y|$) can be estimated by $\Delta x = g\Delta y$ (where $g = \sqrt{\alpha/\beta} = 1.58$). Importantly, there is a $\pi/2$

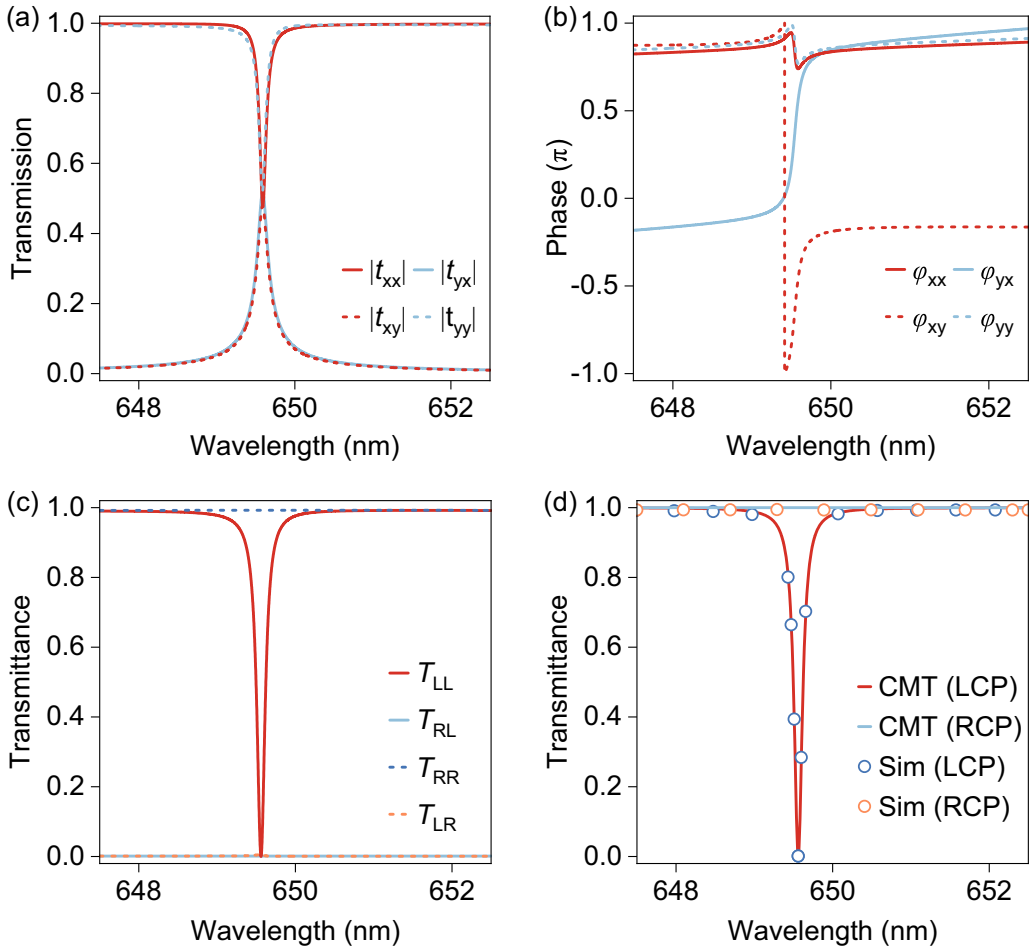

FIG. 4. (a) The transmission and (b) phase spectra under normal-incident linearly polarized light for $\Delta x = 70$ nm and $\Delta y = 45$ nm. The corresponding transmittance spectra of (c) all components of the circularly polarized light, (d) RCP and LCP light.

phase difference between m_x and m_y because the quasi-BIC is aligned to a transmissive Fabry-Perot background and the structure lacks z-axis mirror symmetry [37].

In the following, the cooperation perturbations are considered to manipulate the quasi-BIC transforming from the linear polarization base into circular polarization base (i.e., chiral quasi-BIC). We first calculated the amplitudes and phases of the structure under linearly polarized incidence, as shown in Figs. 4(a) and 4(b). Here, we choose $\Delta x = 70$ nm and $\Delta y = 45$ nm, which approximately satisfy the select law $\Delta x = 1.58\Delta y$. It can be found that the amplitudes of the copolarization and crosspolarization transmission coefficients are identical $|t_{xx}| = |t_{yx}| = |t_{yy}| = |t_{xy}|$ at the quasi-BIC resonance wavelength. Meanwhile, their phase differences at the quasi-BIC resonance wavelength satisfy $\varphi_{xx} = \varphi_{yy}$, $\varphi_{yy} - \varphi_{yx} = \pi/2$ and $\varphi_{yx} - \varphi_{xy} = \pi$. These results fully satisfy the condition of Eq. (3). And then we calculated, using the above parameters, the transmittance spectrum for circularly polarized incidence, as shown in Fig. 4(c). The RCP light is fully transmitted with the same handedness, whereas the LCP light is directly reflected. At the resonant wavelength of $\lambda = 649.56$ nm, the CD reaches near unity, 0.995. As shown in Fig. 4(d), the simulated results can also be well fitted by the analytical model using Eq. (12).

In prior publications there exists an inherent limit between the Q factors and CD of the chiral quasi-BIC, i.e., an increase in the asymmetric parameters on the one hand leads to an increase in the CD, but on the other hand, an exponential increase in the radiation loss [35,37,38,44,60]. However, this limitation can be broken in our design. According to the above discussion, the intrinsic chirality of the quasi-BIC can be maintained as long as the two perturbations Δx and Δy are changed cooperatively. The Q factor of the chiral quasi-BIC resonance in the designed planar chiral structure can be, in principle, continuously boosted, while the amplitude of the CD remains near unity, as shown in Fig. 5(a). What is more, the inherent linkage between Δx and Δy for the maximal intrinsic chirality can be theoretically predicted by $|m_x| = |m_y|$, following a linear relationship of $\Delta x = g\Delta y$ (fitted by blue line), which is confirmed by simulation results in Fig. 5(b). Here, the scale factor is related to the mode profile and could take different values for different chiral quasi-BICs. When the associated perturbations Δx and Δy are small, the Q factor of quasi-BIC roughly scales with the inversely quadratic square of all the perturbations [13,41]: $Q \sim 1/(\Delta x^2 + g^2\Delta y^2)$. The simulated results agree with the formula very well, as depicted by the red line in Fig. 5(b). In the present design, the Q factors of quasi-BICs cover from 4×10^3 to 2.8×10^5, which

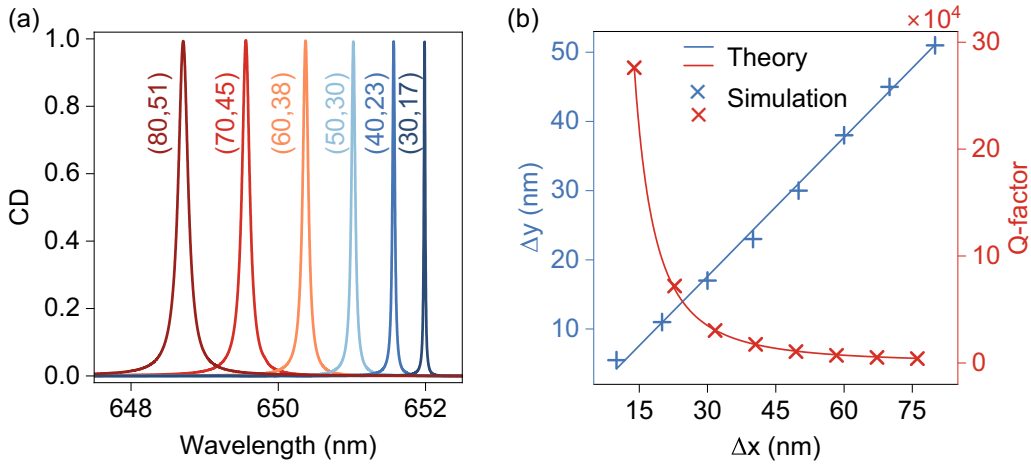

FIG. 5. (a) The CD of the chiral quasi-BIC as functions of the cooperative change of perturbations Δx and Δy. (b) The simulated and theoretically predicted relation between Δx and Δy for maximizing CD and Q factor of the chiral quasi-BIC resonance.

corresponds to the FWHM of CD spectra from 0.16 to 0.02 nm. When considering the experiment, the chiral quasi-BIC with a Q factor of $\sim 10^3$ is feasible [41,44]. Also, the angular dependence of the chiral quasi-BIC resonances is discussed in Fig. S1 of the Supplemental Material [61].

IV. CONCLUSIONS

In conclusion, we propose a straightforward method to achieve the extreme intrinsic chirality in planar structures through manipulating the quasi-BIC *via* in-plane perturbation, and we demonstrate it in a two-dimensional waveguide grating composed of a dimeric grating and a waveguide layer. The CMT is initially employed to derive the conditions necessary for achieving maximal intrinsic chirality in lossless structures. Benefiting from the precise control of the introduced in-plane perturbation to the coupling of quasi-BIC with linearly polarized waves, the high-Q guided mode resonance corresponding to the quasi-BIC is excited within the transparent spectral range of the structure and coupled with x- and y-polarized waves with the same intensity but a phase difference of $\pi/2$, ultimately resulting in the attainment of the extreme intrinsic chirality. The simulation results demonstrate the quasi-BIC exhibits strong interaction with LCP light while decoupling from RCP light, with a CD value of 0.995. Importantly, by adjusting the magnitude of the in-plane asymmetry, the Q factors of the chiral quasi-BIC are independently manipulated, exceeding nearly two orders of magnitude while the CD is maintained at near unity. It should be pointed out that the mechanism for realization of chiral quasi-BICs with tunable Q factors is universal and can be applied to other chiral waveguide grating structures (see detailed information in Fig. S2 of the Supplemental Material [61], for example). Our work provides a simple but powerful paradigm of achieving strong chiral light-matter interactions on an easily fabricated platform, which could offer the possibility of designing high-performance spin-selective optical devices such as chiral emitters, sensors, photonic circuits, etc.

ACKNOWLEDGMENTS

This work was supported by the National Natural Science Foundation of China (Grants No. 12064025, No. 11604136, No. 12304420, No. 12264028, No. 12364045, and No. 12204552), the Natural Science Foundation of Jiangxi Province (Grants No. 20212ACB202006, No. 20232BAB201040, and No. 20232BAB211025), the Young Elite Scientists Sponsorship Program by JXAST (Grant No. 2023QT11), and the Innovation Fund for Graduate Students of Jiangxi Province (Grant No. YC2022-B019).

[1] W. T. B. Kelvin, *The Molecular Tactics of a Crystal* (Clarendon Press, Oxford, UK, 1894).

[2] G. Palermo, G. E. Lio, M. Esposito, L. Ricciardi, M. Manoccio, V. Tasco, A. Passaseo, A. De Luca, and G. Strangi, Biomolecular sensing at the interface between chiral metasurfaces and hyperbolic metamaterials, ACS Appl. Mater. Interfaces **12**, 30181 (2020).

[3] Y. Zhao, A. N. Askarpour, L. Sun, J. Shi, X. Li, and A. Alù, Chirality detection of enantiomers using twisted optical metamaterials, Nat. Commun. **8**, 14180 (2017).

[4] P. Lodahl, S. Mahmoodian, S. Stobbe, A. Rauschenbeutel, P. Schneeweiss, J. Volz, H. Pichler, and P. Zoller, Chiral quantum optics, Nature (London) **541**, 473 (2017).

[5] J. K. Gansel, M. Thiel, M. S. Rill, M. Decker, K. Bade, V. Saile, G. von Freymann, S. Linden, and M. Wegener, Gold helix photonic metamaterial as broadband circular polarizer, Science **325**, 1513 (2009).

[6] A. G. Mark, J. G. Gibbs, T.-C. Lee, and P. Fischer, Hybrid nanocolloids with programmed three-dimensional shape and material composition, Nat. Mater. **12**, 802 (2013).

[7] Z. Wang, H. Jia, K. Yao, W. Cai, H. Chen, and Y. Liu, Circular dichroism metamirrors with near-perfect extinction, ACS Photonics **3**, 2096 (2016).

[8] M. Decker, M. Ruther, C. Kriegler, J. Zhou, C. Soukoulis, S. Linden, and M. Wegener, Strong optical activity from twisted-cross photonic metamaterials, Opt. Lett. **34**, 2501 (2009).

[9] S. Zhang, J. Zhou, Y.-S. Park, J. Rho, R. Singh, S. Nam, A. K. Azad, H.-T. Chen, X. Yin, A. J. Taylor *et al.*, Photoinduced handedness switching in terahertz chiral metamolecules, Nat. Commun. **3**, 942 (2012).

[10] G. Hu, M. Wang, Y. Mazor, C.-W. Qiu, and A. Alù, Tailoring light with layered and moiré metasurfaces, Trends Chem. **3**, 342 (2021).

[11] C. W. Hsu, B. Zhen, J. Lee, S.-L. Chua, S. G. Johnson, J. D. Joannopoulos, and M. Soljačić, Observation of trapped light within the radiation continuum, Nature (London) **499**, 188 (2013).

[12] S. I. Azzam and A. V. Kildishev, Photonic bound states in the continuum: From basics to applications, Adv. Opt. Mater. **9**, 2001469 (2021).

[13] K. Koshelev, S. Lepeshov, M. Liu, A. Bogdanov, and Y. Kivshar, Asymmetric metasurfaces with high-q resonances governed by bound states in the continuum, Phys. Rev. Lett. **121**, 193903 (2018).

[14] M. Kang, T. Liu, C. T. Chan, and M. Xiao, Applications of bound states in the continuum in photonics, Nat. Rev. Phys. **5**, 659 (2023).

[15] I. A. M. Al-Ani, K. As'Ham, L. Huang, A. E. Miroshnichenko, and H. T. Hattori, Enhanced strong coupling of TMDC monolayers by bound state in the continuum, Laser Photonics Rev. **15**, 2100240 (2021).

[16] C. W. Hsu, B. Zhen, A. D. Stone, J. D. Joannopoulos, and M. Soljačić, Bound states in the continuum, Nat. Rev. Mater. **1**, 16048 (2016).

[17] Y. Yang, C. Peng, Y. Liang, Z. Li, and S. Noda, Analytical perspective for bound states in the continuum in photonic crystal slabs, Phys. Rev. Lett. **113**, 037401 (2014).

[18] Z. F. Sadrieva, I. S. Sinev, K. L. Koshelev, A. Samusev, I. V. Iorsh, O. Takayama, R. Malureanu, A. A. Bogdanov, and A. V. Lavrinenko, Transition from optical bound states in the continuum to leaky resonances: Role of substrate and roughness, ACS Photonics **4**, 723 (2017).

[19] P. Wang, F. He, J. Liu, F. Shu, B. Fang, T. Lang, X. Jing, and Z. Hong, Ultra-high-q resonances in terahertz all-silicon metasurfaces based on bound states in the continuum, Photonics Res. **10**, 2743 (2022).

[20] H. M. Doeleman, F. Monticone, W. den Hollander, A. Alù, and A. F. Koenderink, Experimental observation of a polarization vortex at an optical bound state in the continuum, Nat. Photonics **12**, 397 (2018).

[21] S. Li, C. Zhou, T. Liu, and S. Xiao, Symmetry-protected bound states in the continuum supported by all-dielectric metasurfaces, Phys. Rev. A **100**, 063803 (2019).

[22] M. Qin, S. Xiao, W. Liu, M. Ouyang, T. Yu, T. Wang, and Q. Liao, Strong coupling between excitons and magnetic dipole quasi-bound states in the continuum in WS_2-TiO_2 hybrid metasurfaces, Opt. Express **29**, 18026 (2021).

[23] M. Qin, J. Duan, S. Xiao, W. Liu, T. Yu, T. Wang, and Q. Liao, Manipulating strong coupling between exciton and quasibound states in the continuum resonance, Phys. Rev. B **105**, 195425 (2022).

[24] B. Meng, J. Wang, C. Zhou, and L. Huang, Bound states in the continuum supported by silicon oligomer metasurfaces, Opt. Lett. **47**, 1549 (2022).

[25] A. Kodigala, T. Lepetit, Q. Gu, B. Bahari, Y. Fainman, and B. Kanté, Lasing action from photonic bound states in continuum, Nature (London) **541**, 196 (2017).

[26] M. Wu, S. T. Ha, S. Shendre, E. G. Durmusoglu, W.-K. Koh, D. R. Abujetas, J. A. Sánchez-Gil, R. Paniagua-Domínguez, H. V. Demir, and A. I. Kuznetsov, Room-temperature lasing in colloidal nanoplatelets via Mie-resonant bound states in the continuum, Nano Lett. **20**, 6005 (2020).

[27] Q. Song, J. Hu, S. Dai, C. Zheng, D. Han, J. Zi, Z. Q. Zhang, and C. T. Chan, Coexistence of a new type of bound state in the continuum and a lasing threshold mode induced by Pt symmetry, Sci. Adv. **6**, eabc1160 (2020).

[28] L. Carletti, K. Koshelev, C. De Angelis, and Y. Kivshar, Giant nonlinear response at the nanoscale driven by bound states in the continuum, Phys. Rev. Lett. **121**, 033903 (2018).

[29] S. Xiao, M. Qin, J. Duan, F. Wu, and T. Liu, Polarization-controlled dynamically switchable high-harmonic generation from all-dielectric metasurfaces governed by dual bound states in the continuum, Phys. Rev. B **105**, 195440 (2022).

[30] T. Liu, M. Qin, F. Wu, and S. Xiao, High-efficiency optical frequency mixing in an all-dielectric metasurface enabled by multiple bound states in the continuum, Phys. Rev. B **107**, 075441 (2023).

[31] L. Xu, K. Zangeneh Kamali, L. Huang, M. Rahmani, A. Smirnov, R. Camacho-Morales, Y. Ma, G. Zhang, M. Woolley, D. Neshev, and A. E. Miroshnichenko, Dynamic nonlinear image tuning through magnetic dipole quasi-BIC ultrathin resonators, Adv. Sci. **6**, 1802119 (2019).

[32] S. Feng, T. Liu, W. Chen, F. Wu, and S. Xiao, Sum-frequency generation from etchless lithium niobate empowered by dual quasi-bound states in the continuum, Sci. China Phys. Mech. Astron. **66**, 124214 (2023).

[33] C. Huang, C. Zhang, S. Xiao, Y. Wang, Y. Fan, Y. Liu, N. Zhang, G. Qu, H. Ji, J. Han *et al.*, Ultrafast control of vortex microlasers, Science **367**, 1018 (2020).

[34] X. Zhang, Y. Liu, J. Han, Y. Kivshar, and Q. Song, Chiral emission from resonant metasurfaces, Science **377**, 1215 (2022).

[35] Y. Lim, I. C. Seo, S.-C. An, Y. Kim, C. Park, B. H. Woo, S. Kim, H.-R. Park, and Y. C. Jun, Maximally chiral emission via chiral quasibound states in the continuum, Laser Photonics Rev. **17**, 2200611 (2023).

[36] H. Li, H. Zhou, G. Wei, H. Xu, M. Qin, J. Liu, and F. Wu, Photonic spin-selective perfect absorptance on planar metasurfaces driven by chiral quasi-bound states in the continuum, Nanoscale **15**, 6636 (2023).

[37] A. Overvig, N. Yu, and A. Alù, Chiral quasi-bound states in the continuum, Phys. Rev. Lett. **126**, 073001 (2021).

[38] M. V. Gorkunov, A. A. Antonov, and Y. S. Kivshar, Metasurfaces with maximum chirality empowered by bound states in the continuum, Phys. Rev. Lett. **125**, 093903 (2020).

[39] M. V. Gorkunov, A. A. Antonov, V. R. Tuz, A. S. Kupriianov, and Y. S. Kivshar, Bound states in the continuum underpin near-lossless maximum chirality in dielectric metasurfaces, Adv. Opt. Mater. **9**, 2100797 (2021).

[40] L. Kühner, F. J. Wendisch, A. A. Antonov, J. Bürger, L. Hüttenhofer, L. de S. Menezes, S. A. Maier, M. V. Gorkunov, Y. Kivshar, and A. Tittl, Unlocking the out-of-plane dimension for photonic bound states in the continuum to achieve maximum optical chirality, Light Sci. Appl. **12**, 250 (2023).

[41] Y. Chen, H. Deng, X. Sha, W. Chen, R. Wang, Y.-H. Chen, D. Wu, J. Chu, Y. S. Kivshar, S. Xiao *et al.*, Observation of intrinsic chiral bound states in the continuum, Nature (London) **613**, 474 (2023).

[42] C. Menzel, C. Rockstuhl, and F. Lederer, Advanced Jones calculus for the classification of periodic metamaterials, Phys. Rev. A **82**, 053811 (2010).

[43] J. Wu, X. Xu, X. Su, S. Zhao, C. Wu, Y. Sun, Y. Li, F. Wu, Z. Guo, H. Jiang *et al.*, Observation of giant extrinsic chirality empowered by quasi-bound states in the continuum, Phys. Rev. Appl. **16**, 064018 (2021).

[44] T. Shi, Z.-L. Deng, G. Geng, X. Zeng, Y. Zeng, G. Hu, A. Overvig, J. Li, C.-W. Qiu, A. Alù *et al.*, Planar chiral metasurfaces with maximal and tunable chiroptical response driven by bound states in the continuum, Nat. Commun. **13**, 4111 (2022).

[45] K.-H. Kim and J.-R. Kim, High-q chiroptical resonances by quasi-bound states in the continuum in dielectric metasurfaces with simultaneously broken in-plane inversion and mirror symmetries, Adv. Opt. Mater. **9**, 2101162 (2021).

[46] Q.-K. Liu, Y. Li, Z. Lu, Y. Zhou, W. M. Liu, X.-Q. Luo, and X.-L. Wang, Steerable chiral optical responses unraveled in planar metasurfaces via bound states in the continuum, Phys. Rev. B **108**, 155410(R) (2023).

[47] J. Li, Z. Yue, J. Li, C. Zheng, Y. Zhang, and J. Yao, Ultra-narrowband terahertz circular dichroism driven by planar metasurface supporting chiral quasi bound states in continuum, Opt. Laser Technol. **161**, 109173 (2023).

[48] Q. Duan, Y. Zeng, Y. Yin, J. Xu, Z. Chen, Z. Hao, H. Chen, and Y. Liu, Photonic crystal slabs with maximal chiroptical response empowered by bound states in the continuum, Photonics Res. **11**, 1919 (2023).

[49] S. Fan, W. Suh, and J. D. Joannopoulos, Temporal coupled-mode theory for the fano resonance in optical resonators, J. Opt. Soc. Am. A **20**, 569 (2003).

[50] W. Suh, Z. Wang, and S. Fan, Temporal coupled-mode theory and the presence of non-orthogonal modes in lossless multimode cavities, IEEE J. Quantum Electron. **40**, 1511 (2004).

[51] K. Konishi, M. Nomura, N. Kumagai, S. Iwamoto, Y. Arakawa, and M. Kuwata-Gonokami, Circularly polarized light emission from semiconductor planar chiral nanostructures, Phys. Rev. Lett. **106**, 057402 (2011).

[52] S. A. Dyakov, V. A. Semenenko, N. A. Gippius, and S. G. Tikhodeev, Magnetic field free circularly polarized thermal emission from a chiral metasurface, Phys. Rev. B **98**, 235416 (2018).

[53] K. X. Wang, Z. Yu, S. Sandhu, and S. Fan, Fundamental bounds on decay rates in asymmetric single-mode optical resonators, Opt. Lett. **38**, 100 (2013).

[54] R. Jin, L. Huang, C. Zhou, J. Guo, Z. Fu, J. Chen, J. Wang, X. Li, F. Yu, J. Chen *et al.*, Toroidal dipole BIC-driven highly robust perfect absorption with a graphene-loaded metasurface, Nano Lett. **23**, 9105 (2023).

[55] W. Shi, J. Gu, X. Zhang, Q. Xu, J. Han, Q. Yang, L. Cong, and W. Zhang, Terahertz bound states in the continuum with incident angle robustness induced by a dual period metagrating, Photonics Res. **10**, 810 (2022).

[56] M. Cotrufo, A. Cordaro, D. L. Sounas, A. Polman, and A. Alù, Passive bias-free non-reciprocal metasurfaces based on thermally nonlinear quasi-bound states in the continuum, Nat. Photon. **18**, 81 (2024).

[57] L. Huang, L. Xu, D. A. Powell, W. J. Padilla, and A. E. Miroshnichenko, Resonant leaky modes in all-dielectric metasystems: Fundamentals and applications, Phys. Rep. **1008**, 1 (2023).

[58] A. C. Overvig, S. C. Malek, M. J. Carter, S. Shrestha, and N. Yu, Selection rules for quasibound states in the continuum, Phys. Rev. B **102**, 035434 (2020).

[59] P. Yu, A. S. Kupriianov, V. Dmitriev, and V. R. Tuz, All-dielectric metasurfaces with trapped modes: Group-theoretical description, J. Appl. Phys. **125**, 143101 (2019).

[60] Y. Tang, Y. Liang, J. Yao, M. K. Chen, S. Lin, Z. Wang, J. Zhang, X. G. Huang, C. Yu, and D. P. Tsai, Chiral bound states in the continuum in plasmonic metasurfaces, Laser Photonics Rev. **17**, 2200597 (2023).

[61] See Supplemental Material at http://link.aps.org/supplemental/10.1103/PhysRevB.109.205403 for the angular dependence of the chiral quasi-BIC resonances, and for the realization of the chiral quasi-BIC resonances in two-dimensional planar waveguide gratings with different geometric shapes.